Simulation of Induction at Low Magnetic Prandtl Number

Yannick Ponty and Hélène Politano
CNRS, UMR 6202, Observatoire de la Côte d'Azur, BP 4229, Nice Cedex 4, France

Jean-François Pinton
CNRS, UMR 5672, Laboratoire de Physique, École Normale Supérieure, 46 allée d'Italie 69007 Lyon, France
(Received 26 November 2003; published 9 April 2004)

We consider the induction of a magnetic field in flows of an electrically conducting fluid at low magnetic Prandtl number and large kinetic Reynolds number. Using the separation between the magnetic and kinetic diffusive length scales, we propose a new numerical approach. The coupled magnetic and fluid equations are solved using a mixed scheme, where the magnetic field fluctuations are fully resolved and the velocity fluctuations at small scale are modeled using a large eddy simulation (LES) scheme. We study the response of a forced Taylor-Green flow to an externally applied field: topology of the mean induction and time fluctuations at fixed locations. The results are in remarkable agreement with existing experimental data; a global $1/f$ behavior at long times is also evidenced.

DOI: 10.1103/PhysRevLett.92.144503 PACS numbers: 47.65.+a, 47.27.Eq, 91.25.Cw

One of the strongest motivations in the study of nonlinear effects in magnetohydrodynamics is that electrically conductive flows are capable of dynamo action: the stretching of magnetic field lines by the flow velocity gradients can exceed the (Joule) diffusion. A bifurcation threshold occurs, above which the self-generation of a magnetic field takes place. It has been validated in constrained flows of liquid sodium, which mimic analytical models: the Karlsruhe [1] and Riga experiments [2]. The self-generation of a magnetic field in nonconstrained homogeneous flows is still an open problem actively studied by many groups [3]. In this research, numerical studies have long played an important role. Kinematic dynamo simulations assume a given pattern of a stationary velocity field and study the initial linear growth rate of magnetic field perturbations. They have been used extensively to test the dynamo capacity of flow geometries and proved to be successful at determining the dynamo threshold in the Karlsruhe and Riga experiments [4,5]. They have also shown that dynamo action is a possibility in unconstrained homogeneous flows of the von Kármán type [6,7]. Another numerical approach is to perform direct numerical simulations (DNS) of the full governing equations: the induction equation coupled with the fluid dynamical one by the Lorentz force, the flow being sustained by a given force (or equivalently an average geometry). They have confirmed that dynamo action is present in flows with differential rotations and helicity [8–10]. However, DNS are at present restricted to situations where the magnetic Prandtl number, $\mathrm{Pr}_m = \nu/\lambda$ (where λ is the magnetic diffusivity) is of order 1, i.e., to situations where the smallest scales of the magnetic and velocity fields have the same characteristic size [11]. This is not the case in liquid metals, which have very small magnetic Prandtl number values, e.g., $\mathrm{Pr}_m \sim 10^{-6}$ for liquid gallium and $\mathrm{Pr}_m \sim 10^{-5}$ for liquid sodium. Recall that below the dynamo threshold, a stationary forced flow with a power input ϵ (in watts per kg) has a viscous dissipative scale $\eta_u \sim (\nu^3/\epsilon)^{1/4}$ and a Joule diffusive scale $\eta_B \sim (\lambda^3/\epsilon)^{1/4}$—hence a ratio $\eta_u/\eta_B \sim \mathrm{Pr}_m^{3/4}$. Therefore, at low Pr_m, the magnetic diffusive length scale is very much larger than the velocity dissipative scale. If nonlinear effects are to develop, the magnetic Reynolds number $\mathrm{Re}_m \sim UL/\lambda$ (where U and L represent the characteristic velocity and scale of the flow) must be at least of order 1 and thus the kinetic Reynolds number of the flow, $\mathrm{Re} \sim UL/\nu \sim \mathrm{Re}_m/\mathrm{Pr}_m$, must be very large (turbulence is fully developed). A DNS treatment of such a system is at present out of reach.

In this Letter, we present a new approach for the study of the magnetic induction in large Re — low Pr_m flows; we restrict ourselves to regimes below the dynamo threshold. In this parameter region, the magnetic field "lives" essentially within the large and inertial hydrodynamic scales. We thus propose to treat with a subgrid model the velocity scales which are smaller than the magnetic diffusive length. Schemes using hyperviscosity have previously been used [4,12]. Here, we prefer a large eddy simulation (LES) approach, which has proved very successful for the simulation of turbulent flows with large scale structures and for the modeling of energy transfers [13]. In this hybrid scheme, we solve the induction equation on a fully resolved grid and we use a LES method for the velocity field, with a cutoff scale at the end of the magnetic diffusive range. We consider the response of a conductive fluid to a uniform magnetic field: topology of the mean induced field and spatiotemporal features of the magnetic fluctuations are studied. The chosen flow is a forced Taylor-Green (TG) vortex. It shares many similarities with the experimental von Kármán swirling flows which have already been investigated in DNS near $\mathrm{Pr}_m \sim \mathcal{O}(1)$ [9,10].

In nondimensional form, the incompressible MHD equations have two classical control parameters, the magnetic and kinetic Reynolds numbers, and one has to choose a forcing mechanism that generates the desired values of Re_m and Re. In order to be close to experimental procedures, we fix the driving force and magnetic Prandtl number. Hence, the dynamical time t_0 is set to the magnetic diffusion time scale, i.e., $t_0\lambda/L^2 \sim \mathcal{O}(1)$, where L is a length scale characteristic of the system size. Changes in magnetic diffusivity for real fluids would change that time scale. We write the MHD equations, with constant unit density, as

$$\partial_t \mathbf{u} + \mathbf{u}\cdot\nabla\mathbf{u} = -\nabla P + \mathrm{Pr}_m\nabla^2\mathbf{u} + \mathbf{F} + (\nabla\times\mathbf{b})\times\mathbf{B}, \tag{1}$$

$$\partial_t \mathbf{b} = \nabla\times(\mathbf{u}\times\mathbf{B}) + \nabla^2\mathbf{b}, \tag{2}$$

$$\nabla\cdot\mathbf{u} = 0, \qquad \nabla\cdot\mathbf{b} = 0, \tag{3}$$

where $\mathbf{u}$ is the velocity field, $\mathbf{B} = \mathbf{B}_0 + \mathbf{b}$ is the net magnetic field in the flow, sum of the applied field $\mathbf{B}_0$, and induced field $\mathbf{b}$. Once the amplitude F of the driving force is fixed, the (nondimensional) rms intensity of the velocity fluctuations is $u_{\mathrm{rms}} \sim \sqrt{F}$, the Reynolds number is $\mathrm{Re} \sim \sqrt{F}/\mathrm{Pr}_m$, and the magnetic Reynolds number is $\mathrm{Re}_m \sim \sqrt{F}$. The interaction parameter which measures the ratio of Lorentz force to inertial forces is given by $N \simeq B_0^2/u_{\mathrm{rms}} \sim B_0^2/\sqrt{F}$ and is usually small. The above expressions are only dimensional estimates; in practice, the characteristic flow quantities are computed as mean temporal values from the data; cf. Table I.

TABLE I. Time averaged quantities: $u_{\mathrm{rms}} = \langle\mathbf{u}^2\rangle^{1/2}$, $b_{\mathrm{rms}} = \langle\mathbf{b}^2\rangle^{1/2}$, flow integral scale $l_0 = 2\pi\sum_k E_v(k)/k/\sum_k E_v(k)$, Taylor microscale $l_T \sim l_0\mathrm{Re}_e^{-1/2}$, diffusive scale η_B, and eddy turnover time τ_{NL}. Nondimensional parameters: effective Prandtl number $\mathrm{Pr}_{m_{\mathrm{eff}}}$, kinetic Reynolds number $\mathrm{Re}_e = l_0 u_{\mathrm{rms}}/\nu_{\mathrm{eff}}$ (see text), and magnetic Reynolds number $\mathrm{Re}_m = \mathrm{Pr}_{m_{\mathrm{eff}}} R_e$, Taylor-based Reynolds number $\mathrm{Re}_{l_T} \sim \mathrm{Re}_e^{1/2}$, interaction parameter $N = \mathrm{Re}_m B_0^2/u_{\mathrm{rms}}^2$.

Run	No. $\mathbf{B}_0 = 0.1\hat{\mathbf{x}}$	No. $\mathbf{B}_0 = 0.1\hat{\mathbf{z}}$
TG	$\mathrm{Re} = 9209$	$\mathrm{Re} = 9212$
$k_0 = 1$	$\mathrm{Re}_m = 6.65$	$\mathrm{Re}_m = 6.68$
$F = 3/2$	$\mathrm{Re}_{l_T} = 95.94$	$\mathrm{Re}_{l_T} = 95.96$
128^3 grid points	$\mathrm{Pr}_{m_{\mathrm{eff}}} \sim 7.22\times10^{-4}$	$\mathrm{Pr}_{m_{\mathrm{eff}}} = 7.26\times10^{-4}$
$K_c = k_{\max} - 3$	$N = 8.23\times10^{-3}$	$N = 8.18\times10^{-3}$
$k_{\max} = 64$	$l_0 = 2.338$	$l_0 = 2.337$
$t_{\max} = 410$	$l_T = 0.024$	$l_T = 0.024$
	$\eta_B = 0.565$	$\eta_B = 0.563$
	$\tau_{NL} = 1.217$	$\tau_{NL} = 1.224$
	$u_{\mathrm{rms}} = 2.843$	$u_{\mathrm{rms}} = 2.858$
	$b_{\mathrm{rms}} = 0.061$	$b_{\mathrm{rms}} = 0.064$
	$\max\lvert\mathbf{u}\rvert = 8.211$	$\max\lvert\mathbf{u}\rvert = 8.249$
	$\max\lvert\mathbf{b}\rvert = 0.160$	$\max\lvert\mathbf{b}\rvert = 0.180$

We use a parallelized pseudospectral code in a $[0-2\pi]^3$ periodic box. Time stepping is done with an exponential forward Euler-Adams-Bashford scheme. The LES model is of the Chollet-Lesieur type [13] in which the kinematic viscosity ν is replaced in spectral space by an eddy viscosity. In Eq. (1) the magnetic Prandtl number is then replaced by

$$\mathrm{Pr}_m(k,t) = 0.1[1 + 5(k/K_c)^8]\sqrt{E_v(k=K_c,t)/K_c}. \tag{4}$$

Here K_c is the cutoff wave number of the velocity field, and $E_v(k,t)$ is the one-dimensional kinetic energy spectrum. The effective Prandtl number $\mathrm{Pr}_{m_{\mathrm{eff}}}$ is obtained as the temporal mean of $\mathrm{Pr}_m(0,t)$. Note that the effective fluid viscosity ν_{eff} is of the same magnitude. A consistency condition for our approach is that the magnetic field fluctuations are fully resolved when $2\pi/K_c$ is smaller than the magnetic diffusive scale $\eta_B \sim l_0/\mathrm{Re}_m^{3/4}$, l_0 being the integral scale computed from the kinetic energy spectrum.

The flow is driven by the TG vortex geometry

$$\mathbf{F}_{\mathrm{TG}}(k_0) = 2F\begin{bmatrix}\sin(k_0x)\cos(k_0y)\cos(k_0z)\\ -\cos(k_0x)\sin(k_0y)\cos(k_0z)\\ 0\end{bmatrix}; \tag{5}$$

(k_0, k_0, k_0) is the wave vector that prescribes the velocity large scale (hereafter $k_0 = 1$). The $\mathbf{F}_{\mathrm{TG}}$ and $\mathbf{B}_0$ amplitudes are chosen such that the interaction parameter N remains smaller than 10^{-2}. After an initial transient ($t < 10$) the flow has reached a steady state: the kinetic energy fluctuates less than 3.5% around its mean value. All quantities are tracked up to $t_{\max} = 410t_0$; note that $200t_0$ is of the order of the measurement time in most sodium experiments [14–16]. For comparison, the eddy turnover time $\tau_{NL} \sim l_0/u_{\mathrm{rms}}$ is given in Table I

Figure 1 shows the power spectra of the velocity and magnetic field fluctuations with $\mathbf{B}_0$ applied along the $\hat{\mathbf{x}}$ axis (a direction perpendicular to the rotation axis of the counterrotating eddies of the TG cells). The kinetic energy spectrum exhibits a $k^{-5/3}$ Kolmogorov scaling maintained by the LES scheme. The peak at low wave

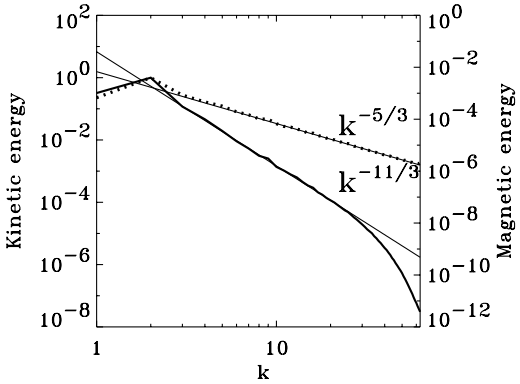

FIG. 1. Magnetic (solid line) and kinetic (dashed line) energy spectra computed at $t = 210$ for Run 1 with $\mathbf{B}_0 = 0.1\hat{\mathbf{x}}$.

number, also visible on the magnetic field spectrum, is due the large scale TG forcing. The magnetic inertial range is well fitted by a $k^{-11/3}$ power law in agreement with a Kolmogorov phenomenology [17,18]. The magnetic diffusive scale is reached within the computational box. The main goal of our numerical strategy is thus achieved: the magnetic fluctuations are fully resolved in a range of scales at which the velocity field follows the Kolmogorov self-similar structure of turbulence. Hence, we get the possibility to study magnetic induction in a fully developed turbulent flow at low magnetic Prandtl number.

Figure 2 displays isosurfaces of the local induced magnetic energy $\langle E_b(\mathbf{x}, t)\rangle_T$ averaged in the time interval $T = [10 - 410]$, shown at 80% of its maximum value. For comparison, we also plot isosurfaces of the induced magnetic energy, $\langle E_{b,\mathrm{lin}}(\mathbf{x}, t)\rangle_T$, obtained numerically from a linear approximation based on time averaged velocities: $\lambda\nabla^2\mathbf{b} = -\mathbf{B}_0\nabla\langle\mathbf{v}(\mathbf{x}, t)\rangle_T$. This is similar to numerical studies based on averaged flow geometries [7,19]. When $\mathbf{B}_0$ is applied along $\hat{\mathbf{z}}$, in a direction parallel to the rotation axis of the TG eddies, the most intense magnetic energy structures are concentrated around the $z = \pi/2, 3\pi/2$ planes, as a result of differential rotation in TG vortices. In this case, the most intense structures of $\langle E_b(\mathbf{x}, t)\rangle_T$ and $\langle E_{b,\mathrm{lin}}(\mathbf{x}, t)\rangle_T$ coincide. For $\mathbf{B}_0$ along the $\hat{\mathbf{x}}$ axis, one observes a concentration of induction around $z = 0, \pi$ planes, as expected from a direct inspection from the flow forcing. Here, the most intense structures of $\langle E_b(\mathbf{x}, t)\rangle_T$ and $\langle E_{b,\mathrm{lin}}(\mathbf{x}, t)\rangle_T$ do not coincide everywhere [see, for example, the location $(\pi/2, \pi/2, 0)$ in Fig. 2(bottom)]. Note that the linear calculation overestimates the time averaged magnetic fluctuations, whatever the orientation of the applied field. Altogether these observations show than one should be cautious when using average velocity fields in the calculation of magnetic induction, particularly if restricted to linear effects. The difference between the fields is probably linked to the large scale electromotive force due to turbulent motions. The influence of this force, as well as the large scale induction topology and its connection with the small scale fluctuations, will be reported in a forthcoming paper [20].

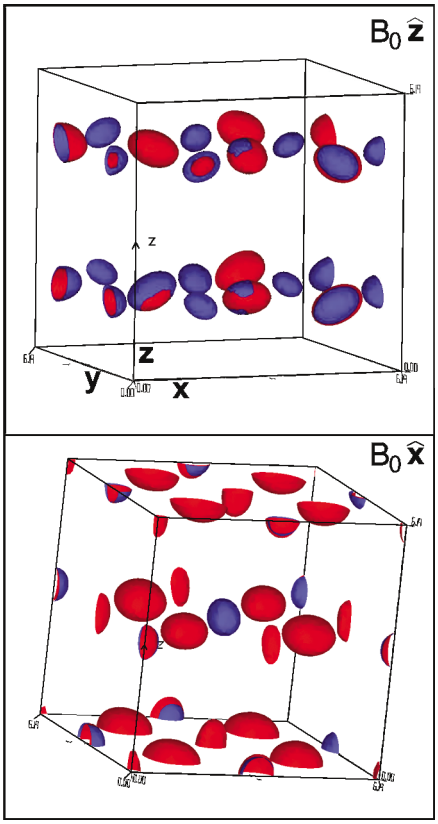

FIG. 2 (color). Topology of the local induced magnetic energy, averaged in time, when $\mathbf{B}_0$ is applied along the $\hat{\mathbf{z}}$ axis (top) and along the $\hat{\mathbf{x}}$ axis (bottom): in red, $\langle E_b(\mathbf{x}, t)\rangle_T$; in blue, $\langle E_{b,\mathrm{lin}}(\mathbf{x}, t)\rangle_T$ (see text). The isosurfaces are plotted at 80% of the maximum values of the fields: $\max\langle E_b\rangle_T = 0.0056$ and $\max\langle E_{b,\mathrm{lin}}\rangle_T = 0.0063$ for $\mathbf{B_0} = 0.1\hat{\mathbf{z}}$, and $\max\langle E_b\rangle_T = 0.0041$ and $\max\langle E_{b,\mathrm{lin}}\rangle_T = 0.0063$ for $\mathbf{B_0} = 0.1\hat{\mathbf{x}}$.

Figure 3 shows the time fluctuations of the induced field amplitude, $|\mathbf{b}(\mathbf{x}, t)|$, probed inside the flow at two locations chosen from the previous topological observations, for $\mathbf{B}_0$ along the $\hat{\mathbf{x}}$ axis. This is equivalent to measurements with local probes as in laboratory experiments. The intensity of the induced magnetic field has strong local fluctuations. The point at $(0, \pi, 0)$ is in a region of strong mean induction, whereas the point at $(0.6\pi, 0.6\pi, 0.6\pi)$ is at location of low mean induction [cf. Fig. 2(bottom)]. We observe that occasionally the induced field gets larger than the applied field. In fact, if small amplitude fluctuations (about 10%) are induced over time intervals of the order of the diffusive time t_0, much larger variations ($\sim$300%) can be observed over long time periods, of the order of $10t_0$. This is in excellent agreement with the experimental observations at comparable Re_m and Pr_m [14–16,18]. In order to be more quantitative, we analyze time spectra; we focus on the case with $\mathbf{B}_0$ applied along the $\hat{\mathbf{x}}$ axis, but the results are identical when $\mathbf{B}_0$ is along $\hat{\mathbf{z}}$. We plot in Fig. 4 the power spectra of time fluctuations of the magnetic field

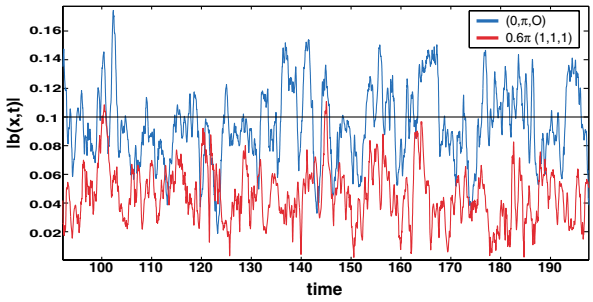

FIG. 3 (color). Time traces of $|\mathbf{b}(\mathbf{x}, t)|$, for $\mathbf{B_0} = 0.1\,\hat{\mathbf{x}}$, at two fixed points. Blue: $(0, \pi, 0)$, mean value $\langle|\mathbf{b}(\mathbf{x}, t)|\rangle_T/B_0 = 0.92$, fluctuation level $|\mathbf{b}(\mathbf{x}, t)|_{\mathrm{rms}}/B_0 = 0.28$. Red: $(0.6\pi, 0.6\pi, 0.6\pi)$, mean value $\langle|\mathbf{b}(\mathbf{x}, t)|\rangle_T/B_0 = 0.44$, fluctuation level $|\mathbf{b}(\mathbf{x}, t)|_{\mathrm{rms}}/B_0 = 0.19$.

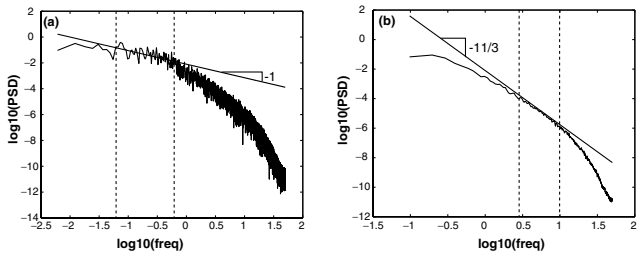

FIG. 4. Power spectral density of the magnetic field fluctuations of $b_x(\mathbf{x}, t)$ in time, recorded at space location $(0, \pi, 0)$, when $\mathbf{B_0} = 0.1\hat{\mathbf{x}}$. (a) PSD computed as averages over Fourier transforms calculated over long time intervals $(164t_0)$ to emphasize the low frequency behavior. (b) PSD estimated from Fourier transforms over shorter time intervals $(10t_0)$. The behavior is identical for the $b_y(\mathbf{x}, t)$ and $b_x(\mathbf{x}, t)$ field components.

component $b_x(\mathbf{x}, t)$ recorded at $(0, \pi, 0)$. The higher end of the time spectrum follows a $f^{-11/3}$ behavior, as can be expected from the spatial spectrum using the Taylor hypothesis of "frozen" field lines advected by the mean flow [18]. For frequencies roughly between $1/t_0$ and $1/10t_0$, the time spectrum develops a $1/f$ behavior, as observed in experimental measurements [15]. Here also, this regime develops for frequencies that are smaller than the one, $1/t_0 \sim 1/\tau_{NL}$, associated with the large scale eddy turnover time (flow forcing). It is not present in the spatial spectrum in Fig. 1, and thus appears as a distinctive feature of the *time dynamics* of the induced field. It is also independent of dynamo action, as has been also observed in the Karlsruhe [16] and Riga [21] experiments . Finally, our numerical study reveals one remarkable feature: the $1/f$ behavior is a global feature. It is observed on the fluctuations of the magnetic energy, as shown in Fig. 5 (as a f^{-2} scaling regime). We thus propose that it results from induction processes which have contributions up to the largest scales in the system. However, the origin of this behavior is not fully understood; it is at present an open problem.

To summarize, the mixed numerical scheme proposed here proves to be a valuable tool for the study of magnetohydrodynamics at low magnetic Prandtl numbers. We have considered here the response to an externally applied field. The time behavior of magnetic field fluctuations is found to be in excellent agreement with experimental measurements. It has also revealed that the $1/f$ regime detected locally traces back to the global dynamics of the flow. Future work will analyze the contribution of turbulent fluctuations to the large scale magnetic field dynamics. We also plan to use this technique to address the question of the variation of the critical magnetic Reynolds number with the magnetic Prandtl number (see, for instance, Marié *et al.* in [3]) or, in a related manner, the existence of a critical magnetic Prandtl number as the kinetic Reynolds number of the flow grows to infinity [11].

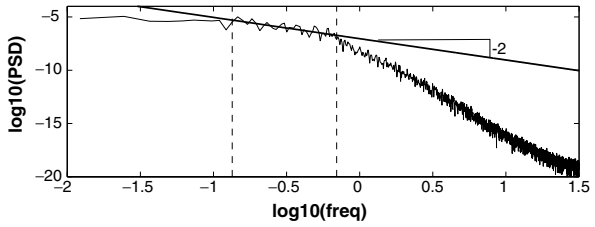

FIG. 5. Power spectral density of the time fluctuations of the magnetic energy $E_b(t) = \langle \mathbf{b}^2(t) \rangle / 2$, integrated over space.

We thank J.-P. Bertoglio, P. Odier, and A. Pouquet for fruitful discussions. This work is supported by CNRS ATIP/SPI, PCMI and GdR-Dynamo. Computations performed on an Alineos PC cluster (OCA) and at IDRIS.

[1] R. Stieglitz and U. Müller, Phys. Fluids **13**, 561 (2001).
[2] A. Gailitis *et al.*, Phys. Rev. Lett. **86**, 3024 (2001).
[3] Special issue on MHD dynamo experiments, Magnetohydrodynamics **38** (2002).
[4] R. Kaiser and A. Tilgner, Phys. Rev. E **60**, 2949 (1999).
[5] A. Gailitis, O. Lielausis, E. Platacis, G. Gerbeth, and F. Stefani, Rev. Mod. Phys. **74**, 973 (2002).
[6] N. L. Dudley and R.W. James, Proc. R. Soc. London, Ser. A **452**, 407 (1989).
[7] L. Marié, J. Burguete, F. Daviaud, and J. Léorat, Eur. Phys. J. B **33**, 469 (2003).
[8] M. Meneguzzi, U. Frisch, and A. Pouquet, Phys. Rev. Lett. **47**, 1060 (1981).
[9] C. Nore, M. Brachet, H. Politano, and A. Pouquet, Phys. Plasmas **4**, 1 (1997).
[10] C. Nore, M.-E. Brachet, H. Politano, and A. Pouquet, *Dynamo Action in a Forced Taylor-Green Vortex*, in Dynamo and Dynamics, a Mathematical Challenge: NATO Science Series II, edited by P. Chossat, D. Armbruster, and I. Oprea (Kluwer Academic, Dordrecht, 2001), Vol. 26, pp. 51-58.
[11] A. A. Schekochihin *et al.*, astro-ph/0308336.
[12] G. A. Glatzmaier and P. H. Roberts, Nature (London) **377**, 203 (1995).
[13] J.-P. Chollet and M. Lesieur, J. Atmos. Sci. **38**, 2747 (1981).
[14] N. L. Peffley, A. B. Cawthorne, and D. P. Lathrop, Phys. Rev. E **61**, 5287 (2000).
[15] M. Bourgoin *et al.* Phys. Fluids **14**, 3046 (2001).
[16] R. Stieglietz and U. Müller, "*The Karsruhe Dynamo Experiment*," Wissenschaftliche Berichte, FZKA Report No. 6756, 2002.
[17] H. K. Moffatt, J. Fluid Mech. **11**, 625 (1961).
[18] P. Odier, J.-F. Pinton, and S. Fauve, Phys. Rev. E **58**, 7397 (1998).
[19] M. Bourgoin, P. Odier, J.-F. Pinton, and Y. Ricard, Phys. Fluids (to be published).
[20] Y. Ponty *et al.*, "Turbulent Fluctuations and Large Scale Magnetic Fields" (to be published).
[21] A. Gailitis *et al.*, Phys. Plasmas **11**, 1 (2004).